LETTERS

Structure of a tetrameric MscL in an expanded intermediate state

Zhenfeng Liu[1,2], Chris S. Gandhi[1] & Douglas C. Rees[1,2]

The ability of cells to sense and respond to mechanical force underlies diverse processes such as touch and hearing in animals, gravitropism in plants, and bacterial osmoregulation[1,2]. In bacteria, mechanosensation is mediated by the mechanosensitive channels of large (MscL), small (MscS), potassium-dependent (MscK) and mini (MscM) conductances. These channels act as 'emergency relief valves' protecting bacteria from lysis upon acute osmotic down-shock[3]. Among them, MscL has been intensively studied since the original identification and characterization 15 years ago[4]. MscL is reversibly and directly gated by changes in membrane tension. In the open state, MscL forms a non-selective 3 nS conductance channel which gates at tensions close to the lytic limit of the bacterial membrane. An earlier crystal structure at 3.5 Å resolution of a pentameric MscL from *Mycobacterium tuberculosis* represents a closed-state or non-conducting conformation[5,6]. MscL has a complex gating behaviour; it exhibits several intermediates between the closed and open states, including one putative non-conductive expanded state and at least three sub-conducting states[7]. Although our understanding of the closed[5,6] and open[8–10] states of MscL has been increasing, little is known about the structures of the intermediate states despite their importance in elucidating the complete gating process of MscL. Here we present the crystal structure of a carboxy-terminal truncation mutant (Δ95–120) of MscL from *Staphylococcus aureus* (SaMscL(CΔ26)) at 3.8 Å resolution. Notably, SaMscL(CΔ26) forms a tetrameric channel with both transmembrane helices tilted away from the membrane normal at angles close to that inferred for the open state[9], probably corresponding to a non-conductive but partially expanded intermediate state.

The full-length SaMscL protein is 120-amino-acid-residues long and shares 40% and 51% homology with *Mycobacterium tuberculosis* MscL (MtMscL, also known as TbMscL) and the *Escherichia coli* MscL (EcMscL), respectively. Initial electrophysiological characterization of SaMscL (ref. 11) established that it exhibited characteristic membrane-tension-dependent MscL activity with significantly shorter open dwell times compared to EcMscL. Excised patches from azolectin liposomes containing SaMscL(CΔ26) show a stereotypical pressure-dependent increase in channel activity, similar to patches containing wild-type EcMscL, with a single channel conductance comparable to EcMscL (Fig. 1). The open state of SaMscL(CΔ26) appears more stable than that of wild-type SaMscL (Fig. 1c, d), suggesting a role for the C-terminal truncation in the gating behaviour change. Nevertheless, as shown in Supplementary Fig. 1, both full-length and SaMscL(CΔ26) are capable of rescuing a mechanosensitive channel knockout strain of *E. coli* cells from osmotic down-shock[12], indicating that they are both functional *in vivo*. Consequently, truncation of 26 residues from the C terminus of SaMscL does not impair its function, consistent with previous reports for EcMscL[13,14].

SaMscL(CΔ26) forms a tetramer in the crystal with the molecular symmetry axis coincident with the crystallographic four-fold axis (Supplementary Fig. 2), so that the asymmetric unit contains one subunit. The SaMscL(CΔ26) tetramer measures ~69 Å wide in diameter and ~37 Å thick (Fig. 2a, b), whereas the MtMscL pentamer, omitting C-terminal residues 102–151 which form a cytoplasmic helical bundle, measures ~52 Å wide and ~50 Å thick (Fig. 2c, d). Excluding the C-terminal residues that have been deleted in SaMscL(CΔ26), the major differences between the amino acid sequences of SaMscL and MtMscL are localized to the periplasmic ends of transmembrane helices TM1 and TM2 and their connecting loop. *In vitro* crosslinking experiments indicate that both CΔ26 and full-length SaMscL are tetrameric in detergent solution and that removal of the C-terminal domain does not change the oligomeric state of SaMscL (Supplementary Fig. 3). Although unexpected, it is not unprecedented that certain multimeric membrane proteins form distinct oligomers in different species. For example, the CorA Mg^{2+} transporter forms a pentamer in *Thermotoga maritima* and a tetramer

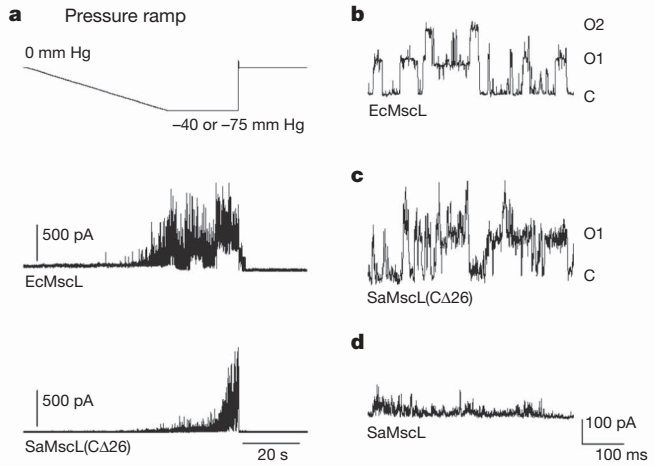

Figure 1 | SaMscL(CΔ26) is a pressure-sensitive channel. a, Pressure-sensitive response of EcMscL and SaMscL(CΔ26) proteins reconstituted into azolectin. Excised patches were held at +60 mV and pressure clamped from 0 to −40 mm Hg (EcMscL) or −75 mm Hg (SaMscL(CΔ26)). In both cases, channel activity steadily increases with greater negative pressure and decreases when the pressure is removed. **b**–**d**, Single channel recordings of EcMscL (**b**), SaMscL(CΔ26) (**c**) and wild-type SaMscL (**d**). EcMscL and SaMscL(CΔ26) channels open and close with discreet jumps in current. Calculated single channel conductances for EcMscL and SaMscL(CΔ26) are 2.9 and 2.6 nS, respectively. In contrast, single channel SaMscL openings flicker rapidly and are too brief to calculate a conductance, as observed previously[11]. C denotes the closed state, whereas O1 and O2 indicate the opening of one and two channels, respectively.

[1]Division of Chemistry and Chemical Engineering, California Institute of Technology, Pasadena, California 91125, USA. [2]Howard Hughes Medical Institute, California Institute of Technology, Pasadena, California 91125, USA.

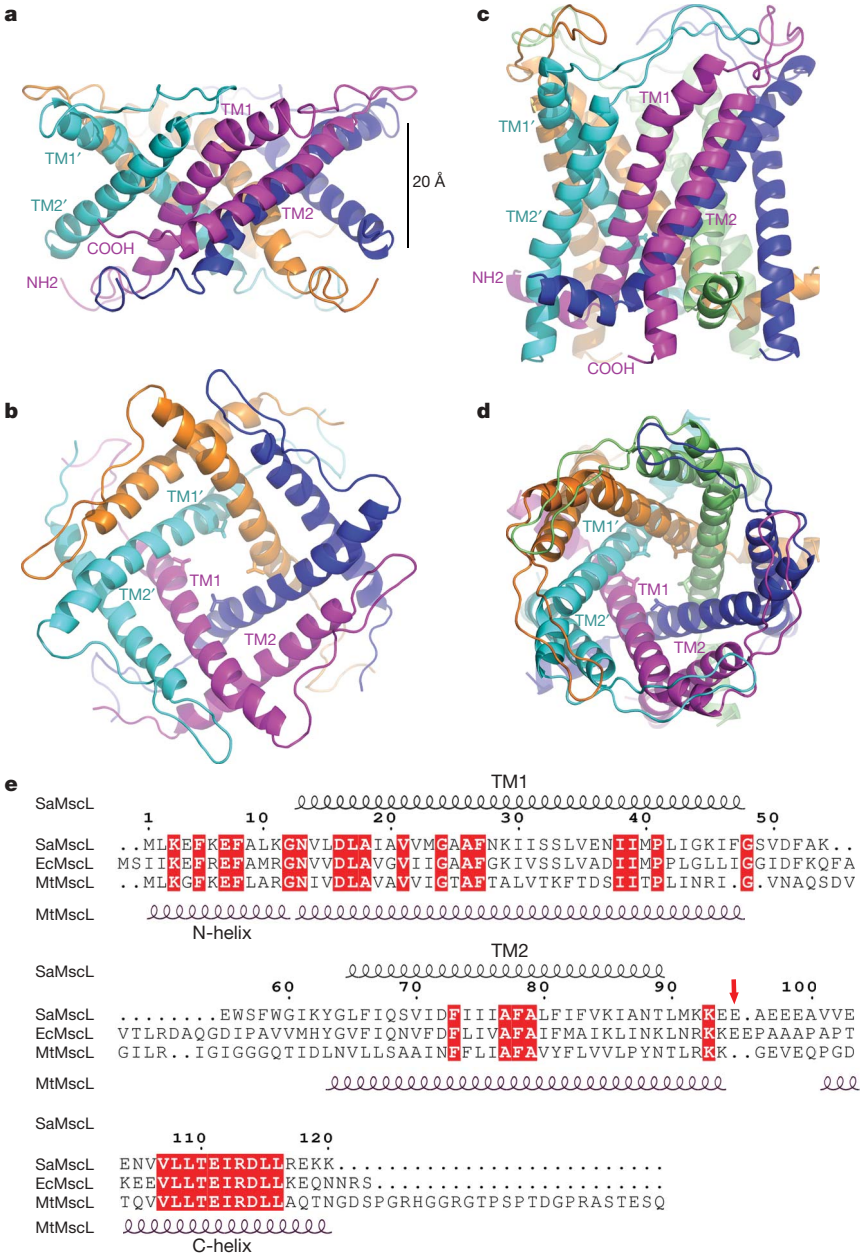

Figure 2 | Structures of SaMscL(CΔ26) and MtMscL. **a**, **b**, The crystal structure of tetrameric SaMscL(CΔ26) viewed along the membrane plane and the pore axis (from the periplasmic side), respectively. **c**, **d**, The membrane-spanning domain of the MtMscL structure (residues 1–101 of Protein Data Bank set 2OAR) viewed as in **a** and **b**. Val 21 is presented as a stick model whereas the polypeptide chains are shown as ribbons. **e**, Structure-based sequence alignment of SaMscL, EcMscL and MtMscL. The red arrow indicates the truncation point (Glu 95) of the SaMscL(CΔ26) mutant.

in *Bacillus subtilis* and *E. coli*[15], whereas the bacterial light-harvesting complex II may be either octameric or nonameric[16]. The ring of c subunits of the membrane-embedded F_0-ATPase also exhibits variable stoichiometry[17].

The secondary structure of the transmembrane region of SaMscL(CΔ26) resembles that of MtMscL (Fig. 2e) with a few exceptions. TM1 of SaMscL(CΔ26) begins at the cytoplasmic surface and extends from Asn 13 to Phe 47, kinking near Pro 41 on the periplasmic side. The polypeptide chain continues through the periplasmic loop from Gly 48 to Gly 64 and crosses the membrane again through TM2 from Leu 65 to Leu 90. TM1 has the same length as in MtMscL, whereas the periplasmic loop and TM2 are four residues and seven residues shorter, respectively, than the corresponding parts of MtMscL. The largest changes in the two structures are the first 12 residues (which adopt an irregular structure in SaMscL(CΔ26) but a short α-helix in MtMscL) and the detailed conformations of the periplasmic loop. In addition, the intrasubunit crossing angle between TM1 and TM2 changes from 134° in MtMscL to 111° in SaMscL(CΔ26) (Fig. 3a, b). An overlay of MtMscL and SaMscL(CΔ26) monomers on TM1 suggests an anticlockwise pivoting of TM2 away from the membrane normal and a translation towards the periplasmic surface (Fig. 3a). In both structures, TM1 and TM2 from the adjacent subunit (TM2′) form an antiparallel pair of helices with crossing angle = 169° and 185° in SaMscL(CΔ26) and MtMscL, respectively. The TM1–TM2′ pair of SaMscL(CΔ26) aligns well with that of MtMscL (root mean square deviation of α-carbon atoms = 1.5 Å) indicating that this pair might move as a rigid body during the conformational change (Fig. 3c and refs 18, 19). The extensive network of largely conserved hydrophobic residues at the TM1–TM2′ interface presumably reflects the stability of this antiparallel helical pair (Supplementary Fig. 4).

The SaMscL(CΔ26) tetramer is ~13 Å thinner along the membrane normal than the membrane-spanning domain of MtMscL pentamer but up to 17 Å wider on the periplasmic surface. The periplasmic surface area of tetrameric SaMscL(CΔ26) is ~2,200 $Å^2$,

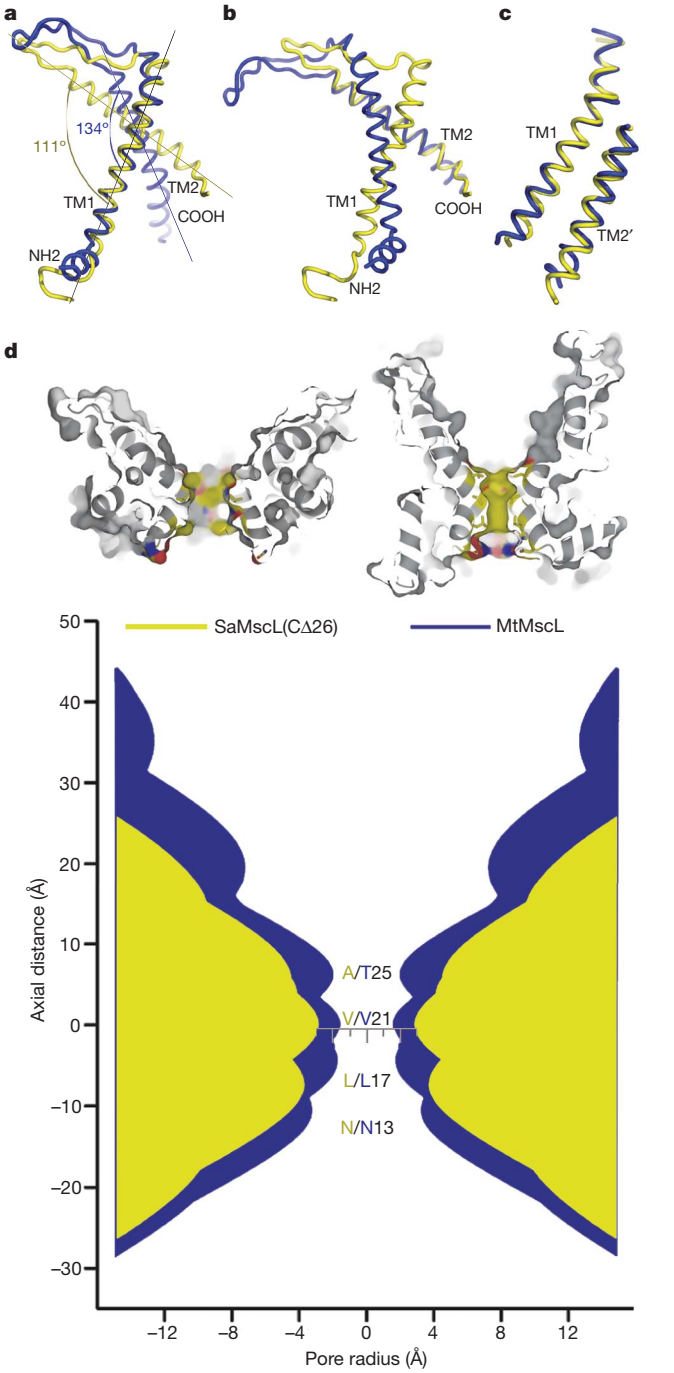

Figure 3 | Alignment of SaMscL(CΔ26) (yellow) and MtMscL (blue). **a**, **b**, Intrasubunit conformational change visualized by aligning the two monomeric structures on TM1 and TM2, respectively. **c**, The superposition of the intersubunit TM1–TM2′ pair from the two structures. **d**, The pore profiles of SaMscL(CΔ26) and MtMscL along the central axes. The top two surface presentations are the sectional views of SaMscL(CΔ26) (left) and MtMscL (right) with the atoms around the constriction coloured in yellow, red and blue for carbon, oxygen and nitrogen, respectively. In the bottom profiles, the regions corresponding to SaMscL(CΔ26) and MtMscL are coloured yellow and blue, respectively. The residues lining the constriction are labelled in the same colour codes.

whereas that of pentameric MtMscL is ~2,000 Å^2. As such, the membrane-spanning region of SaMscL(CΔ26) tetramer is expanded within the membrane plane and compressed along the pore axis as compared to the MtMscL pentamer (Fig. 2a–d). This expansion is also evident in the pore profiles of both channels (Fig. 3d). The constriction of SaMscL(CΔ26) at Val 21 is widened to ~6 Å diameter as compared to ~3 Å in MtMscL. Ala 25 and Leu 17, positioned to either side of Val 21 in the permeation pathway, move farther away from the central axis, opening the pore to ~8 Å around those residues. The corresponding residues in MtMscL, Thr 25 and Leu 17, respectively, lie closer to the axis and hence the pore diameter in this structure narrows to ~4 Å in this region. Although the constriction in SaMscL(CΔ26) is wider than in MtMscL, theoretical studies indicate that hydrophobic pores with diameters less than 9 Å and 13 Å are impermeable to water and ions[20], respectively, implying that both structures are probably non-conducting because they each have narrow and hydrophobic pore constrictions. The expanded state of the channel of SaMscL(CΔ26) reflects the higher tilt angles of TM1 and TM2, relative to the membrane normal. In SaMscL(CΔ26), TM1 and TM2 are tilted 49° and 59° with respect to the pore axis, significantly larger than the 36–38° for the transmembrane helices of MtMscL[6], and close to the angles in an open-state model of EcMscL (~51° for TM1/TM2)[9]. Consequently, the crossing angle between the axes of two adjacent TM1s in SaMscL(CΔ26) (−63°) changes by ~−21° relative to −42° in MtMscL. The combination of the constricted pore and expanded conformation suggests that SaMscL(CΔ26) represents an intermediate state during the transition from the resting closed state to the sub-conducting or open states.

The SaMscL(CΔ26) structure is clearly expanded in the crystal, but why was this conformation trapped? It is possible that removal of 26 residues from the carboxy terminus lowers the energy barrier for the transition from the closed to expanded state and crystal packing facilitates this specific expanded conformation. There are several lines of evidence consistent with this idea. Examination of the MtMscL structure suggests that the C-terminal bundle acts as a plug or pre-filter to the permeation pathway which may dissociate to permit the passage of large solutes, including small proteins[21–23], through the channel. This is consistent with recent electron microscopy work showing that a pore is present at the centre of a gain-of-function mutant (G22N) of EcMscL, whereas the cytoplasmic protrusion is absent[24]. We suggest that the C-terminal helix bundle stabilizes the channel in the closed state and restrains the transmembrane helices from tilting into the expanded conformation. The dissociation of this bundle triggered by the mechanical force transmitted from the lipid bilayer removes the restraint, allowing the transmembrane helices to tilt and transit to the expanded state. Indeed, SaMscL(CΔ26) reconstituted in liposomes is more stable in the open state than the wild-type channel, which displays fast flickering from the closed to open state[11] (Fig. 1c, d), suggesting that the truncation mutant may sample the expanded state more readily under crystallization conditions. The relatively small detergent micelle of *n*-dodecyl-*N*,*N*-dimethylamine-*N*-oxide (LDAO)[25] might also favour the expanded state by exerting curvature stress on the channel.

To model the gating process of MscL, a series of structural models of tetrameric SaMscL from closed to open state was constructed using relationships between the helix tilting angles (η), interhelical-crossing angles (α) and the minimum pore radius (R) of oligomeric channels[26]. We use equations $\cos\alpha = \cos^2\eta + \sin^2\eta\cos\theta$ and $R = d(\tan\eta\ \cot(\alpha/2) - 1)/2$, where $\theta = 360°/N$ with $N = 4$ or 5 for a tetramer or pentamer and d is the helix diameter[26], as the basis for modelling a sequence of tetrameric structures with the α angles determined from various MscL structures in different states. Here we propose a two-step helix-pivoting model of SaMscL gating (see Supplementary movie). In this model, it is assumed that the TM1–TM2′ pair rotates and shifts as a rigid body[18,19]. The first pivoting step occurs during the transition from the closed state to a state near the expanded intermediate (Fig. 4a, b). TM1 pivots clockwise about Val 21 by ~22° and slides along the surface of TM2 (of the same subunit) from Gln 68 down to Ile 75. This induces TM2 to rotate anticlockwise about the pore axis and incline towards the membrane plane along with TM1. Increasing the TM1 tilt angle requires that the helices move farther apart to maintain a symmetric oligomer. As TM2 is in close interaction with TM1 from the next subunit, these movements are synchronized

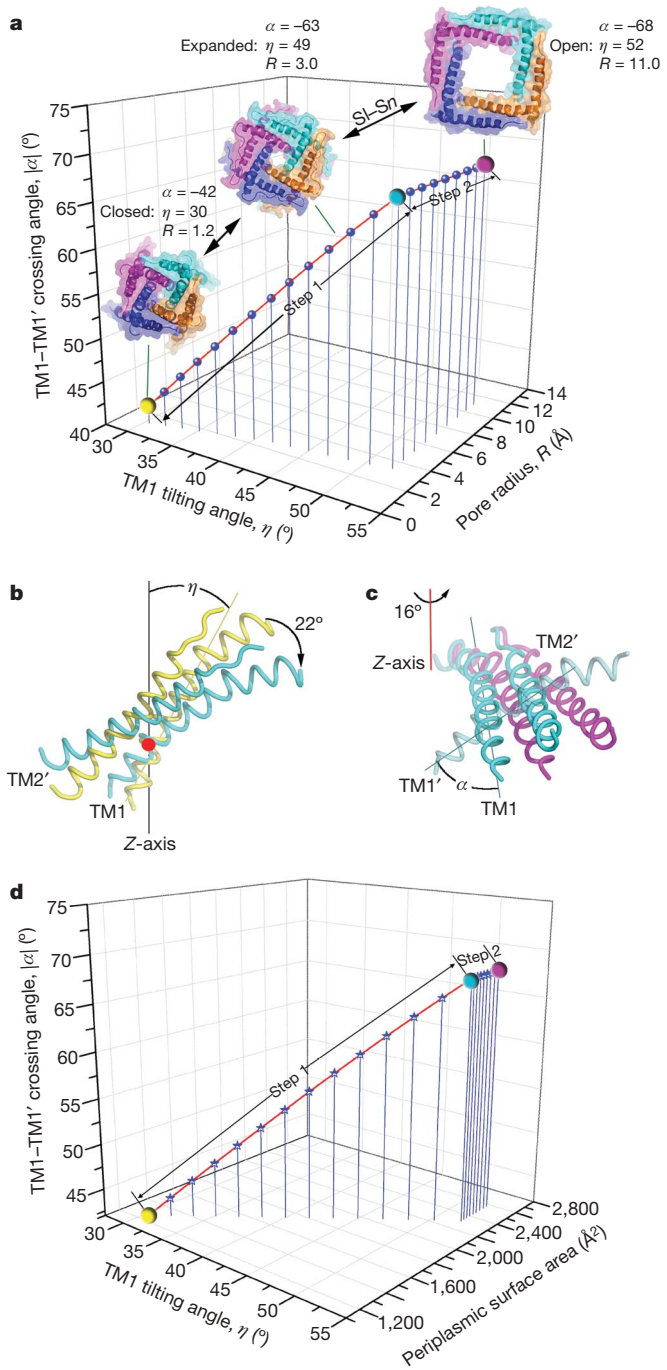

Figure 4 | The two-step helix-pivoting model of SaMscL gating. **a**, The relationship among TM1 tilting angle η, TM1–TM1′ crossing angle α and the pore radius R at Val 21 derived from the gating models. The yellow, cyan and magenta spheres indicate the positions of the resting closed, turning-point intermediate and open states on the curve. S_1–S_n denotes the multiple subconducting states between the expanded and open states. At step 1, η and α are greatly changed due to the helix tilting motion, whereas R is only slightly increased. As the helices swing away from the pore axis at step 2, R increases rapidly, whereas η and α remain constant. **b**, The first pivoting step of TM1–TM2′ occurs about Val 21 (red point). The pair pivots as a rigid body rotating 22° from the resting closed (yellow, based on MtMscL structure[5,6]) to the turning-point intermediate state (cyan, near the SaMscL(CΔ26) structure). **c**, The second pivoting step occurs about the red-line axis through Gly 48, from the intermediate to open state (magenta, based on the Sukharev and Guy model[8]). **d**, The relationship among η, α and the periplasmic surface area of the models. At step 1, the periplasmic surface area expands more drastically than at step 2. See also Supplementary movie.

throughout the tetramer. The crossing angle between two adjacent TM1s increases from −42° to −68° at this stage. This angle reaches −67° in a previous open-state model[8,18] and −55° in an alternative model[9], bracketing the value (−63°) observed in the expanded state structure, suggesting that it is probably near the edge of the open state. At the end of this first step, the periplasmic loop becomes fully stretched between intrasubunit TM1 and TM2, and if tilting continues, the channel would become thinner than the membrane.

The constraint of the membrane thickness leads to a proposed second pivoting step, defined as an anticlockwise rotation by ~16° of the TM1–TM2′ pair about an axis running normal to the membrane and through Gly 48 near the C-terminal end of TM1 (Fig. 4a, c). The highly conserved Gly 48 (Fig. 2e) seems well suited to serve as the pivot for the outward swinging of the TM1–TM2′ pair. This second-step action expands the pore diameter to 22 Å, compatible with the observed large conductance. In MscS, the pore-lining helix also pivots around a glycine residue and moves outwards from the central axis to expand the pore constriction[27]. The periplasmic loop of MscL provides the flexibility for the substantial relative movements of the TM1 and TM2 observed within the same subunit, but also defines the steric limit of channel expansion in the fully open state. Previous functional studies on the periplasmic loop suggested that it may act as a spring, influencing channel kinetics and mechanosensitivity[13,28–30]. During the first step of this transition, the periplasmic surface of SaMscL expands significantly while the channel constriction remains essentially closed until the second step takes place (Fig. 4a, d).

We have determined the crystal structure of a C-terminal truncation mutant of *S. aureus* MscL and demonstrated that SaMscL forms a tetrameric pressure-gated channel. This structure represents a likely expanded intermediate conformation of MscL between the resting closed state and the open state. A two-step helix-pivoting model of the gating mechanism has been proposed.

METHODS SUMMARY

The *Staphylococcus aureus mscL* gene was inserted into a pET15b vector with a stop codon at Glu 95 introduced by site-directed mutagenesis to generate the SaMscL(CΔ26) mutant. The channel was overexpressed in BL21-Gold (DE3) cells and purified in the detergent LDAO by immobilized metal affinity and gel filtration chromatographies. Crystals were grown using the hanging-drop vapour diffusion method. The structure was solved by the method of multiple isomorphous replacement with anomalous scattering.

Crosslinking was performed using *N*,*N*-dicyclohexylcarbodiimide at room temperature for 30 min to 1 h and the products were analysed by SDS-polyacrylamide gel electrophoresis.

The MJF465 (*mscL*$^-$, *mscS*$^-$, *mscK*$^-$) (DE3) strain was used for the osmotic down-shock assay. Cells hosting EcMscL and an empty vector were included as positive and negative control sets, respectively. For the osmotic shock, the culture was diluted 1:500 into sterile double-distilled H_2O. For the mock shock, LB media with 500 mM NaCl was used instead of H_2O.

MscL protein was reconstituted into giant azolectin liposomes via the dehydration/rehydration method and assayed by patch-clamp electrophysiology. Patches containing at least 1–10 channels were excised and currents measured at various pressures. Recording and pipette solutions both contained 200 mM KCl, 40 mM $MgCl_2$, 5 mM HEPES, pH 7.2.

Full Methods and any associated references are available in the online version of the paper at www.nature.com/nature.

Received 15 May; accepted 2 July 2009.
Published online 23 August 2009.

1. Kung, C. A possible unifying principle for mechanosensation. *Nature* **436**, 647–654 (2005).
2. Sukharev, S. & Corey, D. P. Mechanosensitive channels: multiplicity of families and gating paradigms. *Sci. STKE* **2004**, 1–24 (2004).
3. Booth, I. R., Edwards, M. D., Black, S., Schumann, U. & Miller, S. Mechanosensitive channels in bacteria: signs of closure? *Nature Rev. Microbiol.* **5**, 431–440 (2007).
4. Sukharev, S. I., Blount, P., Martinac, B., Blattner, F. R. & Kung, C. A large-conductance mechanosensitive channel in *E. coli* encoded by mscL alone. *Nature* **368**, 265–268 (1994).
5. Chang, G., Spencer, R. H., Lee, A. T., Barclay, M. T. & Rees, D. C. Structure of the MscL homolog from *Mycobacterium tuberculosis*: a gated mechanosensitive ion channel. *Science* **282**, 2220–2226 (1998).

6. Steinbacher, S., Bass, R., Strop, P. & Rees, D. C. in *Current Topics in Membranes. Mechanosensitive Ion Channels, Part A* (ed. Hamill, O. P.) 1–24 (Academic, 2007).
7. Sukharev, S. I., Sigurdson, W. J., Kung, C. & Sachs, F. Energetic and spatial parameters for gating of the bacterial large conductance mechanosensitive channel, MscL. *J. Gen. Physiol.* **113,** 525–540 (1999).
8. Sukharev, S., Betanzos, M., Chiang, C.-S. & Guy, H. R. The gating mechanism of the large mechanosensitive channel MscL. *Nature* **409,** 720–724 (2001).
9. Perozo, E., Cortes, D. M., Sompornpisut, P., Kloda, A. & Martinac, B. Open channel structure of MscL and the gating mechanism of mechanosensitive channels. *Nature* **418,** 942–948 (2002).
10. Anishkin, A. & Sukharev, S. State-stabilizing interactions in the bacterial mechanosensitive channel gating and adaptation. *J. Biol. Chem.* **284,** 19153–19157 (2009).
11. Moe, P. C., Blount, P. & Kung, C. Functional and structural conservation in the mechanosensitive channel MscL implicates elements crucial for mechanosensation. *Mol. Microbiol.* **28,** 583–592 (1998).
12. Levina, N. *et al.* Protection of *Escherichia coli* cells against extreme turgor by activation of MscS and MscL mechanosensitive channels: identification of genes required for MscS activity. *EMBO J.* **18,** 1730–1737 (1999).
13. Blount, P., Sukharev, S. I., Schroeder, M. J., Nagle, S. K. & Kung, C. Single residue substitutions that change the gating properties of a mechanosensitive channel in *Escherichia coli*. *Proc. Natl Acad. Sci. USA* **93,** 11652–11657 (1996).
14. Häse, C. C., Le Dain, A. C. & Martinac, B. Molecular dissection of the large mechanosensitive ion channel (MscL) of *E. coli*: mutants with altered channel gating and pressure sensitivity. *J. Membr. Biol.* **157,** 17–25 (1997).
15. Niegowski, D. & Eshaghi, S. The CorA family: structure and function revisited. *Cell. Mol. Life Sci.* **64,** 2564–2574 (2007).
16. Cogdell, R. J. *et al.* The structure and function of the LH2 (B800–850) complex from the purple photosynthetic bacterium *Rhodopseudomonas acidophila* strain 10050. *Prog. Biophys. Mol. Biol.* **68,** 1–27 (1997).
17. Stock, D., Leslie, A. G. & Walker, J. E. Molecular architecture of the rotary motor in ATP synthase. *Science* **286,** 1700–1705 (1999).
18. Sukharev, S., Durell, S. R. & Guy, H. R. Structural models of the MscL gating mechanism. *Biophys. J.* **81,** 917–936 (2001).
19. Strop, P., Bass, R. & Rees, D. C. Prokaryotic mechanosensitive channels. *Adv. Protein Chem.* **63,** 177–209 (2003).
20. Beckstein, O. & Sansom, M. S. P. The influence of geometry, surface character, and flexibility on the permeation of ions and water through biological pores. *Phys. Biol.* **1,** 42–52 (2004).
21. Cruickshank, C. C., Minchin, R. F., Le Dain, A. C. & Martinac, B. Estimation of the pore size of the large-conductance mechanosensitive ion channel of *Escherichia coli*. *Biophys. J.* **73,** 1925–1931 (1997).
22. Ajouz, B., Berrier, C., Garrigues, A., Besnard, M. & Ghazi, A. Release of thioredoxin via the mechanosensitive channel MscL during osmotic downshock of *Escherichia coli* cells. *J. Biol. Chem.* **273,** 26670–26674 (1998).
23. van den Bogaart, G., Krasnikov, V. & Poolman, B. Dual-color fluorescence-burst analysis to probe protein efflux through the mechanosensitive channel MscL. *Biophys. J.* **92,** 1233–1240 (2007).
24. Yoshimura, K., Usukura, J. & Sokabe, M. Gating-associated conformational changes in the mechanosensitive channel MscL. *Proc. Natl Acad. Sci. USA* **105,** 4033–4038 (2008).
25. Strop, P. & Brunger, A. T. Refractive index-based determination of detergent concentration and its application to the study of membrane proteins. *Protein Sci.* **14,** 2207–2211 (2005).
26. Spencer, R. H. & Rees, D. C. The α-helix and the organization and gating of channels. *Annu. Rev. Biophys. Biomol. Struct.* **31,** 207–233 (2002).
27. Wang, W. *et al.* The structure of an open form of an *E. coli* mechanosensitive channel at 3.45 Å resolution. *Science* **321,** 1179–1183 (2008).
28. Maurer, J. A., Elmore, D. E., Lester, H. A. & Dougherty, D. A. Comparing and contrasting *Escherichia coli* and *Mycobacterium tuberculosis* mechanosensitive channels (MscL). *J. Biol. Chem.* **275,** 22238–22244 (2000).
29. Tsai, I. J. *et al.* The role of the periplasmic loop residue glutamine 65 for MscL mechanosensitivity. *Eur. Biophys. J.* **34,** 403–412 (2005).
30. Ajouz, B., Berrier, C., Besnard, M., Martinac, B. & Ghazi, A. Contributions of the different extramembranous domains of the mechanosensitive ion channel MscL to its response to membrane tension. *J. Biol. Chem.* **275,** 1015–1022 (2000).

Supplementary Information is linked to the online version of the paper at www.nature.com/nature.

Acknowledgements We thank A. Shih for early cloning work, T. Walton for biochemical analysis, A. Lee for initial efforts on the MscL project, J. Choe for expression and purification protocols, O. Lewinson for manuscript reading, Y. Poon and J. Lai for treating MJF465 with λDE3 and the osmotic down-shock assay protocol, J. Kaiser for suggestions on structure refinement, R. Phillips, E. Haswell and P. Pal for discussions, P. Blount for the MJF465 strain, and the staff at SSRL, the Advanced Light Source (ALS) and the Advanced Photon Source (APS) for technical support with crystal screening and data collection. We would like to acknowledge the Gordon and Betty Moore Foundation for support of the Molecular Observatory at Caltech. Operations at SSRL, ALS and APS are supported by the US Department of Energy and NIH. This work was supported in part by grants from the Howard Hughes Medical Institute and the National Institutes of Health (GM084211). C.S.G. was supported in part by postdoctoral fellowships from the National Institutes of Health and the Beckman Foundation. D.C.R. is an Investigator in the Howard Hughes Medical Institute.

Author Contributions Z.L. designed and performed the experiments in molecular biology, biochemistry, crystallography and the structure analysis. Z.L. and C.S.G. conducted the down-shock assays. C.S.G. was responsible for the protein reconstitution and electrophysiology. D.C.R. coordinated the project and contributed to the structure analysis. The manuscript was written by Z.L., C.S.G. and D.C.R.

Author Information The atomic coordinates and structure factors have been deposited at the Protein Data Bank with accession numbers 3HZQ. Reprints and permissions information is available at www.nature.com/reprints. Correspondence and requests for materials should be addressed to D.C.R. (dcrees@caltech.edu).

METHODS

Cloning and protein expression. The gene encoding SaMscL was cloned from genomic DNA by PCR and inserted into a pET15b vector between NdeI and BamHI sites. A stop codon at Glu 95 was introduced using the Quikchange II kit (Stratagene) to create the SaMscL(CΔ26) gene. The plasmid was transformed into BL21-Gold (DE3)-competent cells (Stratagene). A single colony was used to inoculate 200 ml Terrific Broth media with 1% glucose (TB glucose), and the culture was grown overnight at 37 °C with shaking at 225 r.p.m. Two litres of TB glucose media were inoculated with 40 ml of the overnight culture and shaken at 37 °C until the absorbance at 600 nm reached 2.0. Expression was induced with 1 mM IPTG at 30 °C for 2 h, after which the cells were spun down at 6,000*g* and stored at −80 °C.

Protein purification and crystallization. Ten grams of cell pellet were re-suspended in 100 ml lysis buffer (50 mM Tris-HCl, 200 mM NaCl, 44 mM LDAO, pH 8.0). The mixture was sonicated for 4 min in an ice water bath (1 s on and 3 s off) and centrifuged at 17,000 r.p.m. (JA-17, Beckman) for 40 min at 4 °C. The supernatant was applied to a 2-ml Ni-NTA (Qiagen) column by gravity and washed with 10 ml high salt buffer (20 mM Tris-HCl, 300 mM NaCl, 30 mM imidazole, 5 mM LDAO, pH 7.5) and 10 ml low imidazole buffer (20 mM Tris-HCl, 20 mM NaCl, 75 mM imidazole, 5 mM LDAO, pH 7.5). Protein was eluted in 6 ml high imidazole buffer (20 mM Tris-HCl, 20 mM NaCl, 300 mM imidazole, 5 mM LDAO, pH 7.5), concentrated to ~15 mg ml^{-1} in 30 kDa cutoff concentrators (Amicon Ultra-4, Millipore), and loaded onto a Superdex 200 10/30 HR column (GE Healthcare) equilibrated in 10 mM Tris-HCl, 150 mM NaCl, 2 mM LDAO, pH 7.5. The major peak fraction eluting at ~14.3 ml was collected, concentrated to 15–20 mg ml^{-1} protein and used directly for crystallization or frozen in liquid nitrogen for storage at −80 °C.

Crystallization hits for the SaMscL(CΔ26) protein were originally found with the MemGold screen (Molecular Dimensions). Subsequent optimization yielded crystals that matured in a month to a maximum dimension of ~0.5 mm under a condition with 24–30% PEG400, 100 mM Tris-HCl (pH 7.0) and 150 mM Na_2SO_4. The addition of 3.0 mM decyl-β-D-maltoside (DM) to the protein sample improved the crystal size and reproducibility of crystal growth. The diffraction limit was consistently improved from 7 Å to 4.7–4.2 Å resolution, when crystals grown in sulphate were crosslinked with 25% glutaraldehyde through vapour diffusion at 4 °C for 1–2 h according to ref. 31 and then soaked overnight in 10 mM Na_2WO_4 or Na_2MoO_4. For phasing and establishing the sequence register, a series of cysteine mutants of SaMscL(CΔ26) at A9, S32, A87, S57 and S69 were made and crystallized. One crystal of S32C diffracted to 3.8 Å resolution after soaking in a solution of 32% PEG400, 100 mM Tris-HCl (pH 7.0), 20 mM $Na_4P_2O_7$, 200 mM LiCl, 1.8 mM DM, 4.3 mM LDAO and 1.0 mM CH_3HgCl for 4 days. Although this S32C crystal was soaked with CH_3HgCl, the mercury for some reason did not bind to the cysteine residue under this soaking condition. The data set collected from this crystal was used to refine the final structure model reported here.

Data collection and structure determination. Native 1 data set and native 2 data set (S32C) were collected on BL11-1 and BL12-2 of the Stanford Synchrotron Radiation Lightsource (SSRL), respectively. The Na_2WO_4 anomalous data set was collected on a laboratory RaxisIV++ system (Rigaku). The A87C + CH_3HgCl anomalous data set was collected on SSRL BL12-2.

The initial structure was solved by the method of multiple isomorphous replacement with anomalous scattering. The native 1 data set was collected from a molybdate-soaked crystal, while tungstate-soaked and A87C+Hg crystals provided two derivative data sets with strong anomalous signals. The heavy atom positions were determined with ShelxCDE[32], and SigmaA[33] in the CCP4 suite[34] was used to combine the initial phases output by ShelxCDE, yielding a figure-of-merit (FOM) of 0.495 to an effective resolution of 4.7 Å. After density modification by the DM program[35], the resolution for the phase set was extended to 4.2 Å and the FOM was improved to 0.715. The program O[36] was used for model building and adjusting. The initial model was built using the 4.2 Å resolution experimental map (Supplementary Fig. 2a) with anomalous difference Fourier maps (Supplementary Fig. 2b) calculated for the S32C, S69C and A87C crystals (all with Hg bound) to establish the sequence register. The model was first refined against 4.2 Å resolution data with CNS program version 1.2 (ref. 37) to R_{work}/R_{free} = 0.335/0.359. When the 3.8 Å resolution data became available, the model was further refined against this larger data set. The application of a −160 Å^2 *B*-factor sharpening in the map calculation was helpful to show side-chain electron density. After a few rounds of model adjustment and refinement, R_{work}/R_{free} converged to 0.291/0.312. The final $2F_o - F_c$ electron density is well defined in the transmembrane helices (Supplementary Fig. 2c, d) and the periplasmic loop (supplementary Fig. 2c), which allowed continuous tracing of the polypeptide from Gly 12 to Glu 94. The amino terminus (1–11) has relatively weak density and is modelled as an irregular structure instead of a short helix as in MtMscL. Data collection and structure refinement statistics are summarized in Supplementary Table 1.

Structure analysis and model construction. Procheck[38] Ramachandran plot statistics for the final structure are 70.6%, 27.1%, 2.4% and 0.0% for the most favoured, additional allowed, generously allowed and outlier categories, respectively. The sequence alignment in Fig. 2e was generated with the programs ClustalW[39] and ESPript[40]. Structural images were produced by PyMOL[41]. The HOLE program[42] was used to evaluate the pore radius profile from structural models. The periplasmic surface area of the SaMscL(CΔ26) tetramer was approximated as an octagon enclosed by the α-carbon atoms of Gly 48 and Gly 60, whereas that of MtMscL resembles a circular area enclosed by the α-carbon atoms of Val 48. The structure of MtMscL in the closed state (Protein Data Bank code 2OAR), an intermediate model of EcMscL in dimyristoyl-phosphatidylcholine liposomes (1KYL) and the lysophosphatidylcholine stabilized open-state structure of EcMscL (1KYM) were downloaded from the Protein Data Bank. The open state model of Sukharev and Guy[8] (SG model) was downloaded from the *Nature* website (http://www.nature.com/nature/journal/v409/n6821/extref/409720a0_S3.txt). The inter-TM1 angle was calculated by PROMOTIF[43] or directly measured in O[36]. The inter-TM1 angles (α) for 2OAR (closed state), 1KYL, 1KYM and the SG model were determined to be −42°, −43°, −55° and −67°, respectively. The earlier observation that the crossing angles of the pore-lining helices are similar in the pentameric MscL and tetrameric KcsA[6] indicates that it is feasible to apply the crossing angle data retrieved from a pentameric model to a tetrameric one. To generate the models for the first-step pivoting motion, the TM1–TM2′ pair of the expanded-state structure was aligned to the *Z* axis and then pivoted clockwise about the *X* axis on a point around Val 21 to increase the crossing angle α from −42° to −68° in −2° steps. A program based on the equations reported in ref. 26, which describe the relationship among the TM1–TM1′ crossing angle α, the tilt angle η of TM1 and the minimum pore radius *R*, was used for model building in the first step. The intermediate model generated at $\alpha = -62°$ aligns well with the observed structure of SaMscL(CΔ26). To make the second-step pivoting models, the model at the end point (with $\alpha = -68°$) of the first step was rotated anticlockwise in 2° steps about an axis, passing through the α-carbon atom of Gly 48 and parallel to the *Z* axis, using the program PDBSET in CCP4[34].

Crosslinking. Protein was buffer exchanged into 100 mM MES (pH 5.0), 150 mM NaCl, 2 mM LDAO in a 30-kD cutoff concentrator. Reactions with 0.1–1.0 mg ml^{-1} protein and 1–2 mM *N*,*N*-dicyclohexylcarbodiimide (DCCD) were incubated for 30–60 min at room temperature. An equal volume of 2× loading buffer (100 mM Tris-HCl, 4% SDS, 20% glycerol, 0.04% bromophenol blue, 200 mM β-mercaptoethanol, pH 6.8) was added to quench the reaction. The crosslinking products were electrophoretically analysed by 12% SDS-polyacrylamide gel electrophoresis and stained with Coomassie brilliant blue R250. At higher DCCD/protein ratios (Supplementary Fig. 3 lane b and lane d), a tetramer band dominated the crosslinking reaction of both CΔ26 and full-length SaMscL. Weak bands above the dominant species are probably generated by inter-tetramer crosslinking. Crosslinking with glutaraldehyde gave similar results as DCCD.

***In vivo* functional assay.** MJF465 (*mscL*$^-$, *mscS*$^-$, *mscK*$^-$)[12] cells treated with λDE3 lysogenization kit (Novagen) were transformed with pET15b plasmids containing either EcMscL (positive control), SaMscL, SaMscL(CΔ26), or the empty vector (negative control). The transformants were grown on LB-ampicillin (Amp) plates overnight. The down-shock assay protocol was modified from refs 12, 44. In brief, cells were grown and induced with 1 mM IPTG in LB medium with 500 mM NaCl (LB 500) and diluted 1:500 into sterile double-distilled H_2O (down-shock) or LB 500 (mock shock). The cells were recovered at 37 °C for 20 min and 20 μl of the shocked/mock-shocked culture was combined with 80 μl LB 500, spread onto LB-ampicillin plates and incubated overnight at 37 °C. At least four replicates were performed for each shock/mock shock experiment. The mock shock sets always gave a high percentage of surviving colonies for all constructs, including the empty vector.

Protein reconstitution and electrophysiology. Protein reconstitution, vesicle formation and electrophysiology methods were modified from refs 45 and 46. For reconstitution, 1–18 μg of protein in PBS + 0.05% DDM (w:v) was added to 200 μg of azolectin (Sigma) suspension in PBS. The protein/lipid/detergent mixture was incubated for 1 h at room temperature and an additional 3 h with 60 mg of Bio-Beads (Biorad) to remove DDM. After bead removal, the mixture was ultracentrifuged (160,000*g*, 50 min, 4 °C). The resulting pellet was washed once in DR buffer (200 mM KCl, 10 mM HEPES, pH 7.4) and resuspended in 40 μl of the same buffer. Ten microlitres of suspension was spotted onto the underside of a clean screw cap of the EasyXtal CrystalSupport plate (Qiagen) and dried overnight in a vacuum desiccator, depositing a thin lipid film. The film was wetted with 10 μl of DR buffer, equilibrated against 500 μl reservoir of DR buffer, and rehydrated overnight creating a mixture of uni- and multilamellar giant

vesicles. Two microlitres of this mixture was then loaded into a patch clamp recording chamber for analysis.

Unilamellar vesicles were visually identified and excised using patch pipettes with 3–9 MΩ resistances. Bath and pipette solutions were 200 mM KCl, 40 mM $MgCl_2$, 5 mM HEPES, pH 7.2. An HSPC-1 pressure clamp (ALA Scientific Instruments) was used to apply pressure jumps and ramps. The patches were voltage-clamped at +60 mV and current was recorded using an Axopath 200b amplifer (Molecular Devices) and a 10 kHz sampling frequency. Single channel amplitudes were analysed using Clampfit (Molecular Devices).

31. Lusty, C. A gentle vapor-diffusion technique for cross-linking of protein crystals for cryocrystallography. *J. Appl. Cryst.* **32,** 106–112 (1999).
32. Sheldrick, G. M. A short history of SHELX. *Acta Crystallogr. A* **64,** 112–122 (2008).
33. Read, R. Improved Fourier coefficients for maps using phases from partial structures with errors. *Acta Crystallogr. A* **42,** 140–149 (1986).
34. Collaborative Computational Project, Number 4. The CCP4 suite: programs for protein crystallography. *Acta Crystallogr. D* **50,** 760–763 (1994).
35. Cowtan, K. DM: an automated procedure for phase improvement by density modification. *Joint CCP4 ESF-EACBM Newslett. Protein Crystallogr.* **31,** 34–38 (1994).
36. Jones, T. A., Zou, J. Y., Cowan, S. W. & Kjeldgaard, M. Improved methods for building protein models in electron density maps and the location of errors in these models. *Acta Crystallogr. A* **47,** 110–119 (1991).
37. Brunger, A. T. Version 1.2 of the crystallography and NMR system. *Nature Protocols* **2,** 2728–2733 (2007).
38. Laskowski, R. A., MacArthur, M. W., Moss, D. S. & Thornton, J. M. PROCHECK: a program to check the stereochemical quality of protein structures. *J. Appl. Cryst.* **26,** 283–291 (1993).
39. Larkin, M. A. *et al.* Clustal W and Clustal X version 2.0. *Bioinformatics* **23,** 2947–2948 (2007).
40. Gouet, P., Courcelle, E., Stuart, D. I. & Metoz, F. ESPript: analysis of multiple sequence alignments in PostScript. *Bioinformatics* **15,** 305–308 (1999).
41. DeLano, W. L. *The PyMOL User's Manual* (Delano Scientific, 2002).
42. Smart, O. S., Neduvelil, J. G., Wang, X. N., Wallace, B. A. & Sansom, M. S. P. HOLE: a program for the analysis of the pore dimensions of ion channel structural models. *J. Mol. Graph. Model.* **14,** 354–360 (1996).
43. Hutchinson, E. G. & Thornton, J. M. PROMOTIF–a program to identify and analyze structural motifs in proteins. *Protein Sci.* **5,** 212–220 (1996).
44. Iscla, I., Wray, R. & Blount, P. On the structure of the N-terminal domain of the MscL channel: helical bundle or membrane interface. *Biophys. J.* **95,** 2283–2291 (2008).
45. Häse, C. C., Le Dain, A. C. & Martinac, B. Purification and functional reconstitution of the recombinant large mechanosensitive ion channel (MscL) of *Escherichia coli*. *J. Biol. Chem.* **270,** 18329–18334 (1995).
46. Sukharev, S. I., Martinac, B., Arshavsky, V. Y. & Kung, C. Two types of mechanosensitive channels in the *Escherichia coli* cell envelope: solubilization and functional reconstitution. *Biophys. J.* **65,** 177–183 (1993).